

## Full paper

## Role of aluminum and HMTA in the hydrothermal synthesis of two-dimensional n-doped ZnO nanosheets

Gonzalo Murillo<sup>a,\*</sup>, Edgardo Leon-Salguero<sup>a,b</sup>, Paulina R. Martínez-Alanis<sup>c</sup>, Jaume Esteve<sup>a</sup>, Josefina Alvarado-Rivera<sup>b</sup>, Frank Güell<sup>c</sup><sup>a</sup> Instituto de Microelectrónica de Barcelona (IMB-CNM (CSIC)), Campus UAB, 08193, Bellaterra, Barcelona, Spain<sup>b</sup> Posgrado en Nanotecnología, Departamento de Física, Universidad de Sonora, 83000, Hermosillo, Sonora, Mexico<sup>c</sup> ENFOCAT-IN2UB, Universitat de Barcelona, C/Martí i Franquès 1, 08028, Barcelona, Catalunya, Spain

## ARTICLE INFO

## Keywords:

ZnO  
Two-dimensional  
2D nanostructure  
Nanosheet  
Nanocrystal  
Hydrothermal growth  
HMTA  
AlN  
AZO

## ABSTRACT

This work reports the study of the processes behind the growth of two-dimensional (2D) n-doped ZnO nanostructures on an AlN layer. We have demonstrated that AlN undergoes a slow dissociation process due to the basic controlled environment promoted by the hexamethylenetetramine (HMTA). The  $\text{Al}(\text{OH})_4^-$  ions created inhibits the growth along the c-axis, effectively promoting the fast formation of a planar geometry selectively grown on top of the AlN layer. With the use of this promoting layer and a standard hydrothermal method, a selective area growth is observed with micrometric resolution. In addition, by using several advanced characterization techniques such as, X-ray diffraction (XRD), energy-dispersive X-ray spectroscopy (EDS/EDX), X-ray photoelectron spectroscopy (XPS) and photoluminescence (PL), we observed a resulting doping with aluminum of the ZnO nanostructures, occupying substitutional and interstitial sites, that could lead to new promising applications. These high-quality n-doped ZnO nanosheets (NSs) exhibit strong ultraviolet emission in the 385–405 nm region without broad deep level emission. The piezoelectric nature of these nanostructures has been demonstrated by using piezoresponse atomic force microscope (PFM) and with the support of a piezoelectric test device. Therefore, this low-cost and fast selective-area synthesis of 2D n-doped ZnO NSs can be applicable to other aluminum based materials and paves the way to new promising applications, such as bioelectronic applications, energy generation or self-powered sensing.

## 1. Introduction

Zinc oxide (ZnO) is a semiconductor with a direct band gap of 3.36 eV at 300 K (26.85 °C) [1], and an exciton energy of 60 meV [2]. This metal oxide grows into a crystalline wurtzite structure, which is basically two intertwined atomic hexagonal structures of both zinc and oxygen ionic species. This structural characteristic in ZnO produces an asymmetry making the structure highly polarized along c-axis. This asymmetry has two important consequences, a preference for growth along the polarized axis [0001], and a strong piezoelectric response parallel to that growth axis [3], making it an intrinsic piezoelectric material. Additionally, ZnO also shows a strong response in the UV region and excellent electron transport properties. Besides being a biocompatible oxide [4] due to its practically null toxicity, ZnO is a promising material for being used in biological self-sufficient implants [5,6], biosensors [7,8], even as a drug delivery medium and biomolecular sensors [9,10].

When ZnO is doped with aluminum, another promising material is obtained, Al:ZnO (AZO). This material maintains most of the favorable characteristics of ZnO such as low toxicity, low-cost synthesis and transparency in the visible region for thin films applications [11]. Moreover, AZO, compared to ZnO, seems to have improved piezoelectric performance in surface acoustic wave (SAW) devices [12]. Also depending on the aluminum doping percentage, its conductivity can be increased, due to higher carrier concentration. The improved electrical and optical properties of AZO make it as a more economical alternative to indium tin oxide (ITO) with comparable performance [13,14]. Also, it is a material extensively used for field emission devices [15], and for solar cells applications [16–18].

ZnO and AZO nanostructures have been used to successfully manufacture devices that take advantage from these material characteristics, such energy harvesting devices [6,19–22], piezoelectric sensors [7,8,23,24] and with improved properties as chemical sensors [25,26]. These different nanostructures are synthesized and deposited using

\* Corresponding author.

E-mail address: [gonzalo.murillo@csic.es](mailto:gonzalo.murillo@csic.es) (G. Murillo).<https://doi.org/10.1016/j.nanoen.2019.04.017>

Received 14 January 2019; Received in revised form 28 February 2019; Accepted 3 April 2019

Available online 06 April 2019

2211-2855/ © 2019 Published by Elsevier Ltd.

different methods such as Chemical Vapor Deposition (CVD) [27], Pulsed Laser Deposition (PLD) or Atomic Layer Deposition (ALD) [28]. However, the preferred method of research is the hydrothermal method, because it is economic, reproducible, scalable, controllable and environmentally friendly [3,29–32].

The hydrothermal method consists of the use of a water soluble salt of zinc, i.e.  $\text{Zn}(\text{NO}_3)_2$  or  $\text{Zn}(\text{CH}_3\text{COO})_2$ , and a basic buffer such as HMTA, at a controlled temperature. The role of this buffer is to promote the generation of controlled small quantities of  $\text{Zn}(\text{OH})_2$  that evolved in an ordered growth of ZnO nanostructures. However, the exact role of the HMTA in the mechanism of growth is still in debate due to its indirect participation in the nucleation of ZnO, the generation of hydroxide ions ( $\text{OH}^-$ ) and the interaction of the less polar faces of the ZnO crystals with the HTMA derived compounds.

In theory, the growth mechanism for the usual nanowire (NW) structure is as follows, HMTA in the solution works as a basic buffer, it hydrolyses slowly with temperature, according to literature [33–36]. Dissociated zinc nitrate in aqueous solution forms  $\text{Zn}^{2+}$  ions. However, once the solution pH is above 5.5, it starts forming different compounds of  $\text{OH}^-$ , i.e.  $\text{Zn}(\text{OH})_n^m$  ( $n = 2, 4$  and  $m = 2-n$ ), according with the availability of  $\text{OH}^-$  ions in the solution. These compounds are known for participating in the formation of ZnO.

Published research has demonstrated that for concentration ratios of ( $\text{Zn}(\text{NO}_3)_2$ )/[HMTA] around 0.66 (i.e. a solution richer in HMTA) the axial growth is faster. This means that HMTA reduces the radial growth and favors the growth in the axial direction, by restricting the growth along the non-polar, chargeless m-planes, and favoring the growth in the direction of the strongly charged polar c-axis. Ultimately, this results in longer and thinner NWs. When a ZnO seed is used, HMTA also affects the nucleation process by interacting with this seed. Experiments had shown that by increasing the HMTA proportion, the pH of the solution increases, and accordingly, the  $\text{Zn}^{2+}$  ions concentration decreases, resulting in the reduction of the creation of nucleation sites. Thus, higher HMTA concentrations leads to longer NWs, but the density and width are reduced [33,36–39]. It has been shown that the substrate can influence the growth of the nanostructures by the hydrothermal method [40–42], inhibiting the growth or on the other way, improving uniformity, density or growth time. Usually this also can be achieved by a ZnO pre-seeding treatment on the substrate.

AlN is a semiconductor with wurtzite structure and lattice parameters  $a = 0.311$  nm and  $c = 0.497$  nm [43], closely similar to ZnO. From these similarities with ZnO, we expected that AlN could be a good candidate as seed layer to grow well-aligned, high-quality NWs. Instead, 2D nanostructures, ZnO NSs, were grown over a seed layer of AlN, as published by Murillo et al. [40]. Surprising, the growth recipe was exactly the same than the one used to grow ZnO NWs, with the only difference of replacing the gold or ZnO seed layer by an AlN thin film. Our results suggest us that AlN could be playing a more important role leading to the aluminum doping of the ZnO nanostructures (i.e. AZO).

This work analyzes the mechanism of AZO NS growth over  $\text{SiO}_2/\text{Ti}/\text{Pt}/\text{AlN}$  substrates in which, most of the AlN participates as reagent in the growth of the AZO NSs. A uniform forest of high aspect-ratio NSs and even higher volume to area ratio material is generated. Photoluminescence (PL) studies, piezoelectric measurements, chemical and structural characterization were carried out to clarify the exact AlN and HMTA roles. From our results, it seems that the HMTA concentration and the thickness of the AlN substrates determine the structural, optical and piezoelectric properties of the obtained nano-materials.

## 2. Methods

All the chemical products were used as the fabricant sold without previous purification. The zinc nitrate hexahydrate, HMTA, acetone, isopropyl and ethanol were purchased from Sigma Aldrich.

### 2.1. $\text{SiO}_2/\text{Ti}/\text{Pt}/\text{AlN}$ deposition of silicon substrates

First, (100) silicon wafers were submitted to a chemical deposition process to grow a silicon dioxide ( $\text{SiO}_2$ ) layer of 2  $\mu\text{m}$ . Then, Ti/Pt layers of 10nm/50 nm were deposited by sputtering, followed by an AlN thin film with three different thicknesses of 100, 200 and 300 nm. All the substrates were washed with acetone, isopropyl (IPA), ethanol at 98% (EtOH) and deionized water (DIW).

### 2.2. AZO NS synthesis

The growth solution of zinc nitrate hexahydrate at 98% [ $\text{Zn}(\text{NO}_3)_2 \cdot 6\text{H}_2\text{O}$ ] and metanamine at 98% (HMTA) [ $\text{C}_6\text{H}_{12}\text{N}_4$ ] were mixed in DIW in equimolar solution of 5 mM. After that, 100 ml of solution were poured into a wide mouth amber glass jar, and the substrates were put facing down floating in the solution (i.e. AlN layer was immersed in the solution). Afterwards, the jar was hermetically sealed and placed in a convection oven at a controlled temperature of 80 °C for 3 h. Finally the substrates were washed in DIW, IPA and EtOH and gently dried with  $\text{N}_2$ .

### 2.3. Fabrication of proof-of-concept device

This prototype consists of two metalized cover slips working as electrodes and a sandwiched layer of ZnO NSs in between. Specifically the bottom electrode contains 30 nm of Ti and 20 nm of Pt, and a layer of 100 nm of AlN deposited on top by RF sputtering, followed by the hydrothermal growth of a layer of ZnO NSs (as previously indicated, for 3 h at 80 °C). The top electrode is made by the second cover slip etched with HF to get an irregular topography (with a roughness of  $\sim 200$  nm), cleaned with HCl (37%) and DIW and then metalized with 50 nm of aluminum obtain a zig-zag profile. The cover slip corresponding to the second electrode was then flipped away and put on top of the other cover slip (i.e. bottom electrode and piezoelectric material) facing down to close the electric circuit. The resulting mounted system was placed on top of a rectangular microscope slide to give it robustness. Two cables were connected to each electrode by using silver paste (RS Components). Finally the whole mounted and connected system was cover with a transparent epoxy (Sigma-Aldrich) to provide mechanical robustness and isolation against water.

### 2.4. Structural and chemical analysis

Field-emission scanning electron microscopy (FESEM) and energy dispersive X-ray spectroscopy analysis (EDS/EDX) were performed with a Zeiss AURIGA and an Oxford Inca X-Act, respectively. The samples were placed on a carbon tape for adhesion, samples images were generated with an operating voltage of 1–3 kV and using a secondary electrons detector. EDS/EDX measurements were obtained applying a voltage of 10 kV. X-ray powder diffraction (XRD) spectra of the samples were obtained with a Bruker D8 Advance diffractometer ( $\text{CuK}\alpha$ ,  $\lambda = 1.5418$  Å). A  $2\theta$  angle ranging from 15° to 80°, a voltage of 40 kV, and a current of 40 mA were used.

### 2.5. PL studies

Room-temperature PL measurements were made with a chopped Kimmon IK Series He–Cd laser (325 nm and 40 mW). Fluorescence was dispersed through an Oriel Corner Stone 1/8 74000 monochromator, detected with a Hamamatsu R928 photomultiplier, and amplified through a Stanford Research Systems SR830 DSP lock-in amplifier. A 360 nm filter was used for filtering the stray light. It is worth pointing out that all the emission spectra were corrected using the optical transfer function of the PL setup.

## 2.6. XPS analysis

A PerkinElmer PHI 5100 spectrometer with a dual anode Al/Mg using the Mg K of 1254 eV was used as X-ray excitation source. All spectra were charge shifted using C 1s peak at 284.8 eV as reference. High resolution spectra curve fitting was carried out using a Shirley background subtraction and a Gauss-Lorentz function.

## 2.7. Electrical measurements

Voltage measurements of the piezopotential generated by the prototype were performed by introducing it in an ultrasound bath at 35 kHz (ULTRASONIC LC 20 H, Elma) and measuring the open-voltage output with the electrochemical analyzer CHI1030A (CH Instruments) when alternating the ultrasound activation every 5 s. The electrical connection to read-out the potential was alternated to measure the direct (d) and inverted connection (e) in order to observe the sign change of the piezopotential.

## 2.8. Piezoresponse force microscopy (PFM) measurements

A substrate with ZnO NSs was immersed in ethanol and submitted to ultrasound for 5 min in order to release the NSs from the substrate. A drop of the resulting solution of ethanol and released NSs was deposited on top of a silicon die coated by 20nm/50 nm of Ti/Au. A Digital Instruments MultiMode™ 8 AFM from Bruker with a NanoScope V controller was used to obtain the topography the single NS and measure the piezoresponse on top of it. An AC voltage was applied as driving excitation between the Pt-coated AFM tip (CDTP-NCHR-20) and the conductive substrate at contact mode. The induced mechanical deformation of the sample at the same frequency, due to the inverse piezoelectric effect, was acquired. The effective piezoelectric coefficient is then calculated as the slope of the tip displacement versus the applied bias voltage.

## 3. Results and discussion

Table 1 summarizes the samples studied in this work. All the samples were submitted to the deposition of SiO<sub>2</sub>/Ti/Pt/AlN described in experimental section. Samples 1, 2 and 3, corresponding to an AlN thickness of 100, 200 and 300 nm, respectively, were submitted to the described hydrothermal method used for NS synthesis. For samples 4–7, an AlN thickness of 300 nm was used. Identically to sample 3, sample 4 was dipped in aqueous acid solution of HNO<sub>3</sub> [0.5 M] for 20 s as final step. Sample 5 was also dipped in the same acid solution but no NS synthesis was performed. Samples 6 and 7 were submitted to the same NS synthesis process but without zinc nitrate and HMTA, respectively.

Fig. 1a–g shows FESEM images and EDS/EDX results for samples 1–7, Fig. 1h shows the results for average zinc and aluminum atomic percentage for samples 1–3. After the hydrothermal growth, AZO NSs were obtained with a diameter ranging from 1 to 2 μm and an average thickness of 20 nm. The different AlN thicknesses affect the growth of the NSs, thicker AlN layers give denser NS forests. In addition, samples

2 and 3 show a secondary layer of NS grown on top of the initial NS layer (Fig. 1b–c and S1), despite of using the same growth time (3 h) and temperature (80 °C).

In order to analyze the chemical composition of the AZO NSs by means of EDS/EDX analysis, the nanostructures were released from the substrates, and subsequently collected. For this, samples were put inside EtOH solution, and sonicated for 2 min, to obtain a suspension of released AZO NSs. Then, drop of the resulting solution was applied to a brand-new Si substrate, left it dry at room temperature and repeated six times, to successfully transfer the nanostructures. This was done to avoid the spectra from the remaining AlN in the substrate and have a clear count of the atomic percentage. The results show an increase in the aluminum content with the thickness of the AlN seed layer. Specifically, samples 1, 2 and 3 had an average aluminum atomic percentages of 9.7, 10.6 and 11.4, respectively (Fig. 1h), while zinc percentages, 22.3%, 21.3% and 20.4% correspondingly, decrease as the aluminum percentages increases, indicating an integration of the aluminum atoms by substitution of zinc atoms in the AZO NSs. Interestingly, oxygen content was remained constant at 68% for all the samples.

These results suggest that, in presence of AlN, ZnO nanostructures grow with NS geometry, integrating part of the aluminum ions into the ZnO wurtzite lattice substitutionally. To test this, sample 4 was dipped in an acid solution of HNO<sub>3</sub> [0.5 M] for 20 s the grown AZO NSs. Then, we analyze it by SEM, EDS/EDX and XRD, showing that AlN was fully removed from the substrate, in contrast to sample 5 where the AlN layer does not suffer any significant attack due to the acid treatment (see Fig. 1d and e). From EDS/EDX measurements, it can be inferred that only SiO<sub>2</sub> remain in sample 4, confirming that most of the AlN was integrated into the AZO lattice.

In fact, it is known that AlN decomposes in Al(OH)<sub>3</sub> and Al(OH)<sub>4</sub><sup>-</sup> in presence of water and this reaction is catalyzed by the presence of OH<sup>-</sup> ions, suggesting an interaction between AlN and the HMTA. In order to study this reaction, samples 6 and 7 were submitted to the same NS synthesis conditions of temperature and growth time, but using different nutrient solutions. For sample 6, a solution of HMTA [5 mM] without zinc nitrate was used. In contrast, the nutrient solution for sample 7 was only composed of zinc nitrate [5 mM]. After the synthesis reaction, no nanostructure growth was observed in sample 7. It can be explained because, although AlN reacts with water to release OH<sup>-</sup> ions, the reaction in deionized water is very slow, stating to take place after 24 h [44]. In contrast, in sample 6, AlN is attacked and decomposed in the HMTA solution leaving a porous surface with a different chemical composition (see Fig. 1f). Therefore, HMTA provides a steady source of OH<sup>-</sup> ions which serves as catalyst for the AlN hydrolysis.

We proposed that most of the AlN participates as a reagent in the AZO NS growth, because AlN is dissociated and most of it is integrated into the NSs during the growth process (Fig. 2). Due to the nature of this growth mechanism, in which a group of complex reactions takes place, aluminum is found in form of Al<sup>3+</sup> ions and complex hydroxides which can be integrated into the ZnO crystal lattice and effectively doping it to form AZO.

Fig. 3 shows XRD spectra of the samples studied in this work. AlN

**Table 1**

Growth parameters of the samples. All the samples were growth at standard conditions of 3 h at 80 °C.

Sample	AlN thickness [nm]	Zn(NO <sub>3</sub> ) <sub>2</sub> [5 mM]	HMTA [5 mM]	AZO NSs	Acid Treatment HNO <sub>3</sub> [0.5 M]
1	100	Yes	Yes	Yes	No
2	200	Yes	Yes	Yes	No
3	300	Yes	Yes	Yes	No
4	300	Yes	Yes	Yes	Yes
5	300	No	No	No	Yes
6	300	No	Yes	No	No
7	300	Yes	No	No	No

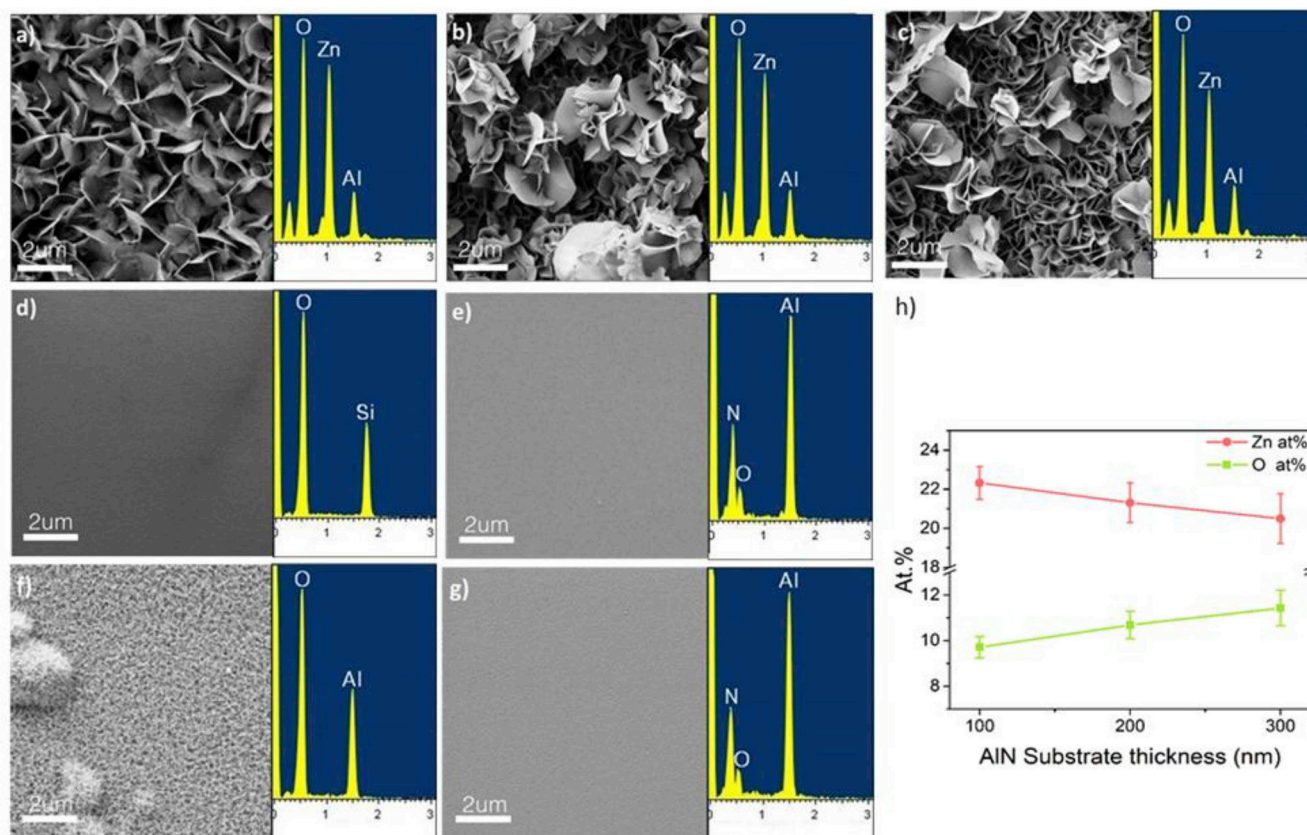


Fig. 1. FESEM and EDS/EDX of a) sample 1, b) sample 2, c) sample 3, d) sample 4, e) sample 5, f) sample 6 and g) sample 7. H) EDS/EDX results showing the atomic percentages of NSs grown on top of different substrates.

signals (red line) of three different AlN thickness (100, 200 and 300 nm) before any treatment and according to PDF#88–2360 AlN (002) peaks were identified. After AZO NS synthesis, AlN peaks had disappeared, leaving ZnO (blue line) for the 3 different AlN substrate thicknesses, showing the characteristic peaks for ZnO agreeable to PDF#36–1451. In this particular case a main diffractions appear at  $2\theta = 34.7^\circ$  (002) (literature  $2\theta = 34.42^\circ$ ) and  $62.1^\circ$  (103) (literature  $2\theta = 68.8^\circ$ ) with no shift or intensity change. The higher intensity of the (002) peak suggests a preferential growth with the c-axis perpendicular to the substrate [45] (see Fig. 2c). In sample 3 as shown in Fig. 3c, additional peaks appeared at  $31.76^\circ$  (100),  $47.49^\circ$  (102),  $56.52^\circ$  (110), presumably due to the incipient secondary grown layer. AZO (001) peak seems to be overlapped with the base substrate signal Pt–Ti. The calculations of the lattice parameters and domain sizes are presented in Table S1 and were calculated using the Scherrer equation and Williamson Hall method [45]. Taking from literature that undoped ZnO lattice parameters are  $a = 0.325$  nm and  $c = 0.520$  nm, the resulting lattice parameters seems to be consistent for the three samples [46].

To further analyze the properties of the AZO NSs, a PL analysis was performed. Fig. 4a shows the results for samples 1, 2 and 3, and an additional sample in which an Au thin film of 50 nm was used as seed layer to obtain un-doped ZnO NWs for comparison. PL results of un-doped ZnO and AZO NSs showed significant changes in the optical properties. It is clear from the spectra that the AZO NSs emit a much stronger UV light, whereas the un-doped ZnO NWs emit weak UV and strong visible light, which is a consequence of the larger surface area of the NWs respect to the NSs [47]. Also, we can observe a clear UV emission shift as the AlN layer thickness increases. The characteristic emission peak for the undoped ZnO NWs at 380 nm (3.27 eV) moves to 385 nm (3.22 eV) for sample 1 (AlN 100 nm), 389 nm (3.19 eV) for sample 2 (AlN 200 nm) and 405 nm (3.06 eV) for sample 3 (AlN 300 nm). This behavior is characteristic for AZO as aluminum content increases [11,16,23,48] and the number of charge carriers increases consequently, improving its conductivity and reducing its band gap. Aluminum can serve as donor in ZnO lattice and decrease the wide band gap, which will improve the electrical and optical properties of

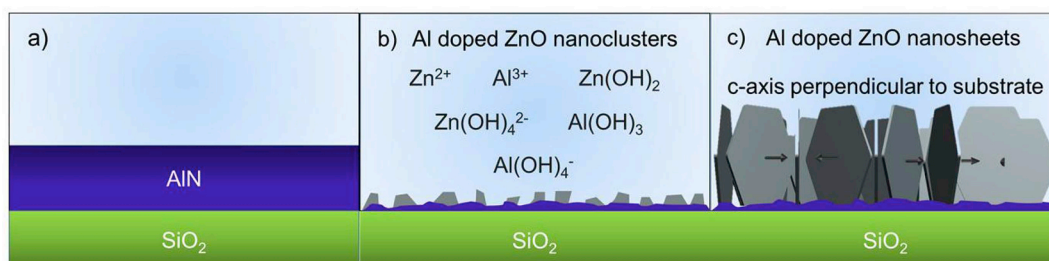
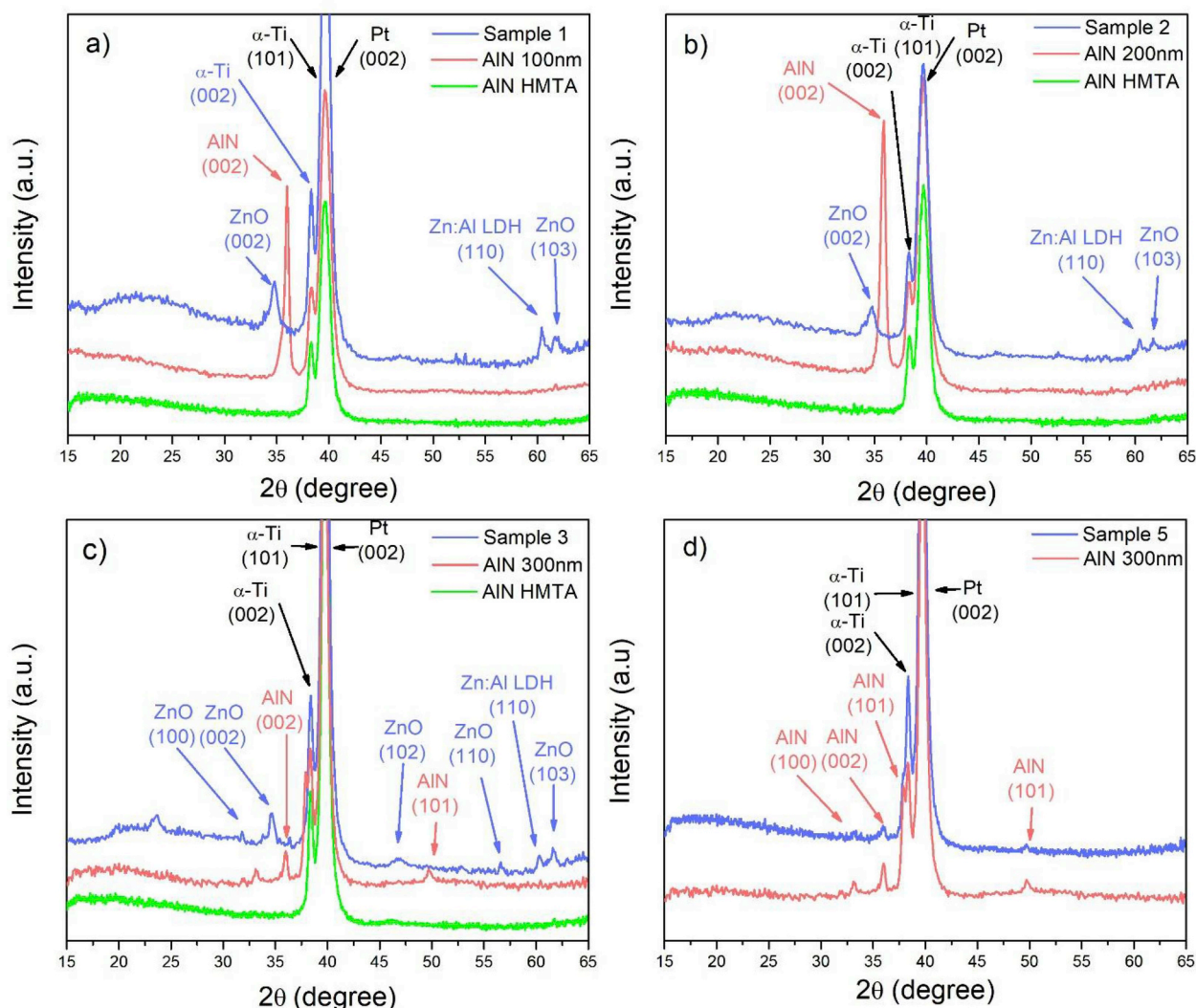


Fig. 2. Growth scheme of the ZnO NSs. A) AlN deposition, b) zinc and aluminum species in water solution, and c) synthesis of the ZnO NSs.



**Fig. 3.** XRD patterns of the samples. a) Sample 1 (blue), AlN 100 nm base substrate (red) and AlN 100 nm substrate after HMTA treatment without zinc (green). b) Sample 2 (blue), AlN 200 nm base substrate (red) and AlN 200 nm substrate after HMTA treatment (green). c) Sample 3 (blue), AlN 300 nm base substrate (red) and AlN 300 nm substrate after HMTA treatment (green). d) Brand-new AlN 300 nm substrate (blue) and AlN 300 nm after acid ( $\text{HNO}_3$ ) treatment (red).

ZnO. This UV redshift can be ascribed to  $\text{Al}_i$  beside the  $\text{Zn}_i$ . This was generated by the substitution of zinc sites with aluminum atoms. This result, together with the fact that the EDS/EDX shows an increase in the aluminum atomic percentage and the XRD shows the characteristic (002) and (103) ZnO peaks, confirm that ZnO wurtzite structure is being doped by aluminum during the growth.

XPS analysis of the ZnO NS coatings was performed to confirm aluminum doping. The samples show Zn  $2p_{3/2}$  and Zn  $2p_{1/2}$  peaks around at 1022.0 and 1045.1 eV (Fig. 4b). Those binding energies correspond to  $\text{Zn}^{2+}$  oxidation state in ZnO wurtzite lattice [49–53]. In Fig. 4c, Al 2p doublet peak is located around 74.0 eV. These positions suggest that  $\text{Al}^{3+}$  ions are forming Al–O bonds in the ZnO lattice, Al 2p core level peak in pure  $\text{Al}_2\text{O}_3$  show higher binding energy values (75 eV) than those observed for AZO films [53,54]. Fig. 4d shows the high resolution spectra of O 1s core level peak. At lower binding energy values a broad satellite peak from a non-monochromated X-ray source was detected. In Table S2 results from peak fitting of the O 1s signal are presented. Three main peaks at 532.6 ( $\text{O}_{\text{III}}$ ), 531.4 ( $\text{O}_{\text{II}}$ ) and 530 ( $\text{O}_i$ ) eV were found and are related to loosely bound oxygen ( $\text{OH}^-$ ), oxygen defects in ZnO and Al–O bonds, and oxygen in the wurtzite lattice, respectively [50–53]. O 1s peak position for Al–O bond in pure alumina appears very near to that of oxygen defects of ZnO as it was not possible

to resolve. However, it is clear that the intensity of  $\text{O}_{\text{II}}$  peak increase for the ZnO growth over the thickest AlN coating, and as it was shown by SEM imaging, the NSs grown more densely compacted over the substrate. At this respect,  $\text{O}_i \times$  below 528 eV is associated to ZnO in contact with the Pt metallic coating that is below the AlN coating. The samples showed some regions where the silicon wafer is exposed because of film cracking, then some photoelectrons from the ZnO growth at the interface possibly escaped to the surface and were detected. Thus, after internal charge reference to C 1s at 284.8 eV, this peak appeared at lower binding energies since no electron flooding gun was used during measurements.

ZnO NW formation is a process that takes place due to the polar charged surfaces along the c-axis, which are intrinsic to the wurtzite crystal structure and are the same that confer this structure with its piezoelectric properties. This structure is formed by interposed planes of polar charged surfaces, the chemically active  $\text{Zn}^{2+}$  terminated (0001) plane, and the inert  $\text{O}_2$  terminated (000–1) surface. During the growth phase,  $\text{OH}^-$  ions provided by the HMTA are attracted to this plane, favoring the growth along that axis and resulting in a long NW structure as proposed in Fig. 5a.

Regarding the proposed NSs synthesis, although AlN in aqueous solution at room temperature forms a hydrophilic aluminum oxide thin

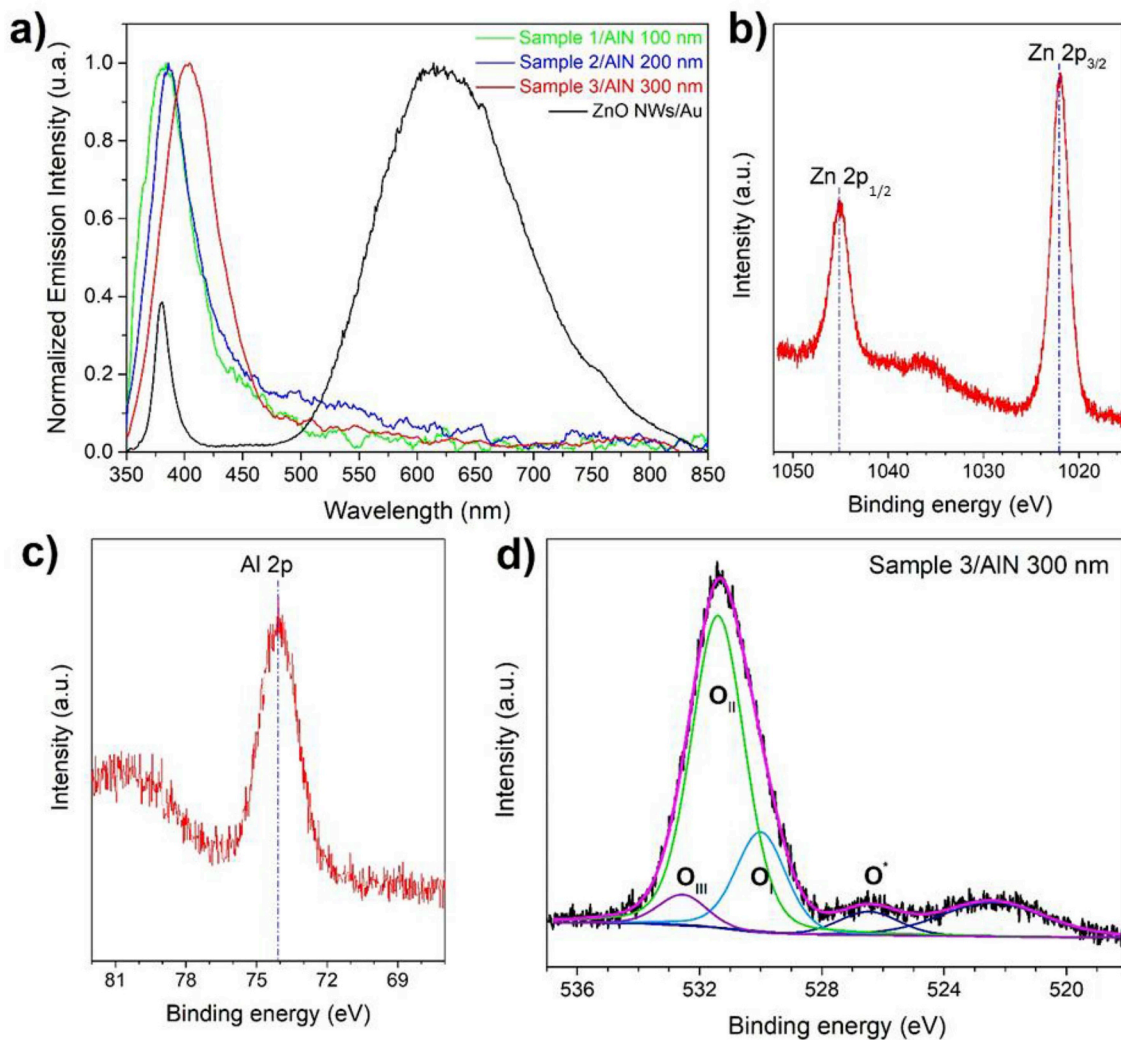
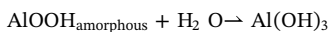


Fig. 4. a) PL spectra of the ZnO NSs and NWs for comparison. b) High resolution XPS spectra of ZnO 2p doublet of zinc in sample 3. c) High resolution XPS spectra of aluminum 2p peak in ZnO NSs in sample 3. d) Curve fitting of the XPS O 1s peak in sample 3.

film that provides chemical protection and preventing a reaction [44], above a temperature of 77 °C, AlN forms amorphous aluminum oxide hydroxide (AlOOH), which in turn start forming Al(OH)<sub>3</sub>. The next reaction taking place under a basic solution [44,55,56]:



When HMTA is in aqueous solution, it creates an alkaline solution, that in contact with AlN, promotes its dissociation, and consequently, the liberation and formation of Al(OH)<sub>4</sub><sup>-</sup>. The Al(OH)<sub>4</sub><sup>-</sup> bonds stronger to the (0001) Zn<sup>2+</sup> ions terminated plane, inhibiting the growth along the c-axis and resulting in a 2D radial growth (Fig. 5b) [31,57]. The quantity of Al(OH)<sub>4</sub><sup>-</sup> present in the medium, increases with the pH that, at the same time, is determined by the HMTA concentration. This result in thinner NSs, due to the little or no growth along the c-axis [57].

It is important to mention that this particular NS geometry cannot be attributed only to the presence of Al<sup>3+</sup> ions. It has been reported aluminum doping of ZnO [58] with the use of Al(NO<sub>3</sub>)<sub>3</sub> as aluminum source, obtaining NWs. This is because Al(NO<sub>3</sub>)<sub>3</sub> dissolves into Al<sup>3+</sup> and 3 nitrate ions in aqueous solution instead of the Al(OH)<sub>4</sub><sup>-</sup>, and for

that reason the c-axis growth inhibition does not take place, thus reinforcing the proposed growth model. In fact, to the best of our knowledge, there are no reports about the growth of nanosheets using only HMTA and zinc nitrate as a mean to increase the pH of the solution. In fact, while there are some reports of NSs structures obtained increasing the pH, this increase was always produced by adding NaOH to the growth solution [30,34,36,59].

In conclusion, by growing ZnO nanostructures on AlN substrates, AlN undergoes a slow dissociation process, due to the basic environment promoted by the HMTA, and consequently the formation of Al(OH)<sub>4</sub><sup>-</sup> ions (see Fig. 5b). This inhibits the growth along the c-axis, effectively promoting the formation of a NS geometry selectively on substrates covered by AlN [40]. The crystal growth is apparently faster radially than axially, as less volume is needed due to 2D geometry of the NSs compared to the 1D one of the NWs. Because the aluminum hydroxide ions availability is localized in areas close to the AlN surface, a selective area growth is observed with micrometric resolution. In addition, it is expected a doping of the ZnO crystal with aluminum atoms, and because of the ionic effective radius of the Al<sup>3+</sup> ions is 53.5 p.m., compared with Zn<sup>2+</sup> ions of 74 p.m. [60], aluminum atoms could occupy substitutional and interstitial sites, expecting the appearance of a ferroelectric effect, which would mean an improvement of the piezoelectric properties after a poling process. This dissociation of AlN is also

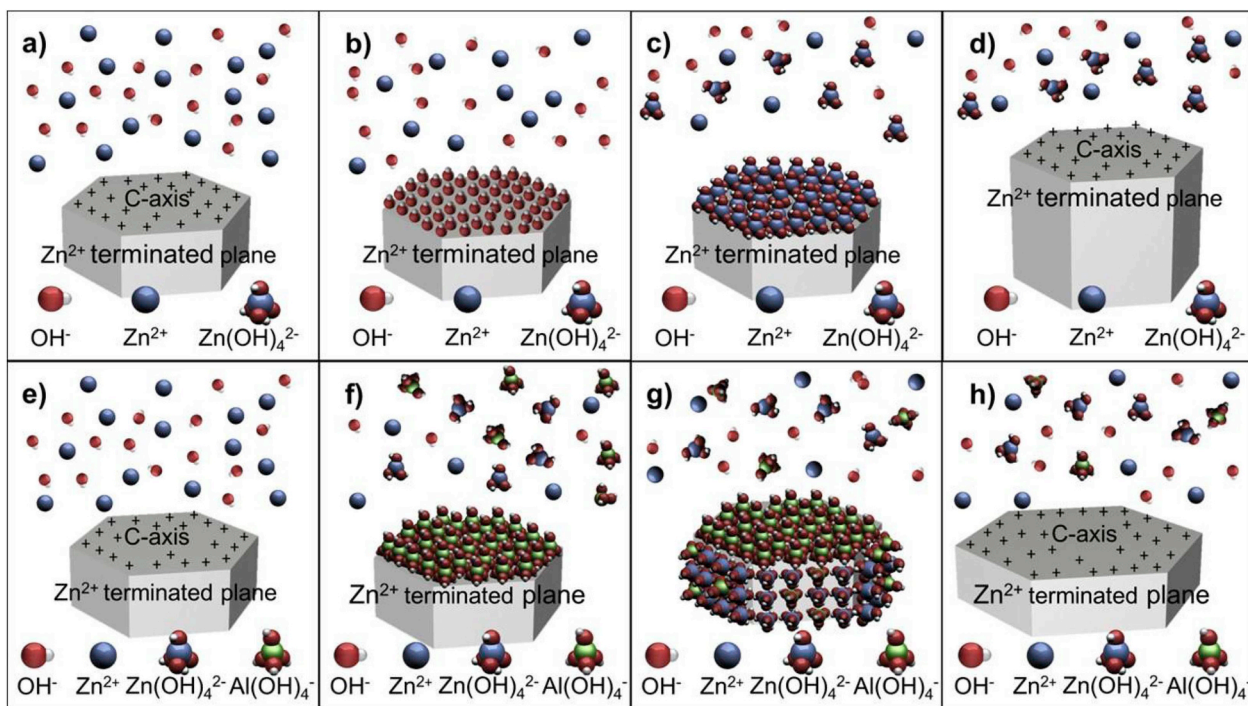


**Fig. 5.** Proposed growth mechanism of the ZnO NW (top): a) equimolar solution HMTA and  $\text{Zn}(\text{NO}_3)_2$ ; b)  $\text{OH}^-$  ions are attracted to the charged polar surface; c)  $\text{OH}^-$  ions combines with  $\text{Zn}^{2+}$  ions to form  $\text{Zn}(\text{OH})_4^{2-}$  ions; and d)  $\text{Zn}(\text{OH})_4^{2-}$  forms ZnO promoting growth along c-axis. Proposed growth mechanism of the ZnO NS (bottom): e)  $\text{Al}(\text{OH})_4^-$  and  $\text{Al}(\text{OH})_3$  rich solution due to AlN hydrolysis; f)  $\text{Al}(\text{OH})_4^-$  ions are strongly attracted to the polar charged surface, screening the  $\text{OH}^-$  ion attachment on that plane; g)  $\text{OH}^-$  ions are weakly attached to the non-polar faces along with some  $\text{Al}^{3+}$  ions; and h) radial growth is promoted and growth along is inhibited, also some aluminum atoms are integrated into the lattice.

demonstrated by the reduction of the AlN thickness after a growth process (Fig. S2) and due to identification of the XRD peak corresponding to AlN (002) which is reduced in Fig. 3a–b and fully removed in Fig. 3c.

The piezoelectric behavior of the ZnO NSs synthesized with this method was tested by using to different alternatives. On one side, a Piezoresponse Atomic Force Microscopy (PFM) was used to measure the effective piezoelectric coefficient of a single NSs (Fig. 6a). A silicon substrate covered with a thin layer of gold was used as ground electrode and a Pt-coated AFM tip probe as top electrode. The calculated piezoresponse of the single ZnO NSs was found to be of around 4 p.m./V (Fig. 6b) [61]. The I–V characteristic shows the typical behavior of a double Schottky diode, suggesting a semiconductor nature (Fig. 6c). One reached the conductivity region, the mean value nanosheet resistivity was found to be  $\sim 435$  MOhms, which proves a low conductivity of the grown n-doped ZnO. On the other side, a test device was fabricated to proof the concept of generating energy by piezoelectric effect when the NSs are deformed. Inspired in Prof. Wang's works [62,63], ZnO nanostructures were grown on top of a metallic substrate (i.e. the bottom electrode) covered by 100 nm of AlN and another metallic substrate, an aluminum coated zig-zag electrode, was placed on top to generate a mechanical deflection on the nanostructures and collect the generated charges. The whole device, depicted in Fig. 6d, was wired and encapsulated with epoxy and immersed in an ultrasound bath where it was submitted to alternate ultrasound activation (every 5 s). The resulting output piezopotential was measured with a potentiostat set up to measure open-circuit voltage with an input impedance of  $1 \times 10^{12}$  Ohms. A voltage amplitude of  $> 1$  V was measured (Fig. 6e) when ultrasounds were activated and the electrode connection was inverted to demonstrate the piezoelectric nature of the signals, which change their sign depending on the connection polarity (Fig. 6f). The open-circuit current was also measured and shown in Fig. 6g. By applying higher forces on top of the generator, making sure full contact between NSs and the electrode, a value of around 1  $\mu\text{A}$  was

obtained which suggests a promising high power density. These both alternative characterizations demonstrated the piezoelectric nature of the ZnO NSs grown by this method and using a buffer AlN layer. In addition, we demonstrated that nanosheets, due to their piezoelectric nature, biocompatibility, reduced thickness and high aspect ratio, can be used to electrically stimulate cells due to the electromechanical interaction with them [61]. Therefore, this nanomaterial has been found to be a great candidate for electroceutical applications, where chemical drugs are proposed to be replaced by electrical stimulating devices [64,65].

#### 4. Conclusions

In summary, we have proposed and experimentally verified a mechanism of hydrothermal growth of high-quality n-doped ZnO planar nanostructures on a substrate covered by an AlN layer. We have proven that AlN suffer a slow dissociation process due to the buffered basic environment created by the HMTA present in the nutrient solution. The resulting  $\text{Al}(\text{OH})_4^-$  ions inhibits the growth along the c-axis, consequently promoting a selective-area growth of 2D n-doped ZnO NSs on top of the AlN layer. In order to demonstrate this process, we have used different characterization techniques such as XRD, EDS/EDX, XPS and PL. These results show aluminum doping of the ZnO nanostructures occupying substitutional and interstitial sites, supporting our theory about the AlN dissociation. The resulting aluminum doped ZnO NSs have been demonstrated to be piezoelectric with an effective piezoresponse of 4 p.m./V. Due to their high aspect ratio and flexibility, they generated more than 1 V of output voltage when mechanically activated with ultrasounds. We have observed this effect with substrates covered by aluminum and  $\text{Al}_2\text{O}_3$  and it is extensible to other aluminum based compounds. This growth procedure opens doors to low-cost and fast selective-area growth of 2D ZnO crystals that could lead to new promising applications such as bioelectronics, energy generation and self-powered sensing [61,66–69].

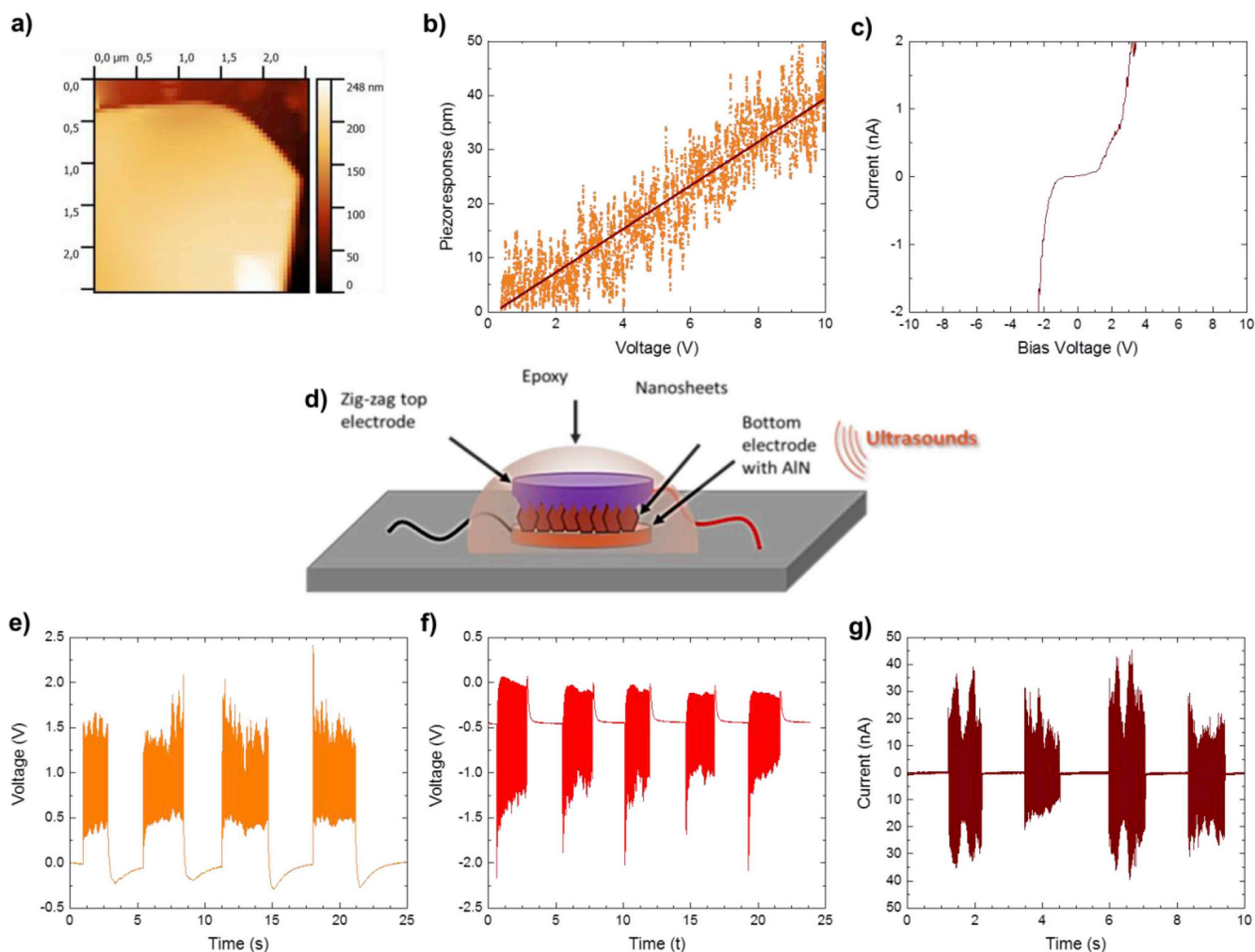


**Fig. 6.** a) AFM topography of a ZnO NS. b) Piezoresponse measured by PFM and I-V curve of a single ZnO NS. d) Diagram illustrating the proof-of-concept device composed of a cover slip working as bottom electrode with a layer of ZnO NSs hydrothermally grown for 3 h at 80 °C on top of 100 nm of AlN and a top electrode made by another cover slip etched and metalized to obtain a zig-zag profile; Open-circuit voltage measurements after encapsulating the device with epoxy and introduce it in an ultrasound bath, by using e) direct and f) inverted electrode connections. In addition, g) the open-circuit current flow was measured for the same conditions.

### Author contributions

The manuscript was written through contributions of all authors. All authors have given approval to the final version of the manuscript. Dr. G. Murillo and E. Leon-Salguero contributed equally to this work.

### Acknowledgments

This work was supported by EnSO project (H2020-ECSEL-JU, contract number: 692482) and NG4Cell project (TEC2015-72461-EXP). P. R. Martínez-Alanis and F. Güell are grateful to project MAT2017-87500-P and to the Programa Ajut a la Recerca Transversal de l'IN2UB 2018 for financial support. Finally, we want to thank H. Lozano and N. Domingo for measuring the piezoresponse of the ZnO NS, and M. Duque and A. Aranda for the electrical characterization of the proof-of-concept device.

### Abbreviations

ALD	Atomic Layer Deposition
AZO	Aluminum-doped ZnO
CVD	Chemical Vapor Deposition
DIW	deionized water

EDS/EDX	energy-dispersive X-ray spectroscopy
EtOH	ethanol
FESEM	Field-emission scanning electron microscopy
HMTA	hexamethylenetetramine
IPA	isopropyl
ITO	indium tin oxide
NS	nanosheet
NW	nanowire
PL	photoluminescence
PLD	Pulsed Laser Deposition
SAW	Surface Acoustic Wave
XPS	X-ray photoelectron spectroscopy
XRD	X-ray diffraction

### Appendix A. Supplementary data

Supplementary data to this article can be found online at <https://doi.org/10.1016/j.nanoen.2019.04.017>.

### References

- [1] P. Rodnyi, I. Khodyuk, Optical and luminescence properties of zinc oxide (Review), *Optic Spectrosc.* 111 (2011) 776–785, <https://doi.org/10.1134/S0030400X11120216>.

- [2] B.P. Zhang, N.T. Binh, Y. Segawa, K. Wakatsuki, N. Usami, Optical properties of ZnO rods formed by metalorganic chemical vapor deposition, *Appl. Phys. Lett.* 83 (2003) 1635–1637, <https://doi.org/10.1063/1.1605803>.
- [3] L. Vayssieres, K. Keis, A. Hagfeldt, S.E. Lindquist, Three-dimensional array of highly oriented crystalline ZnO microtubes, *Chem. Mater.* 13 (2001) 4395–4398, <https://doi.org/10.1021/cm011160s>.
- [4] Z. Li, R. Yang, M. Yu, F. Bai, C. Li, Z.L. Wang, Cellular level biocompatibility and biosafety of ZnO nanowires, *J. Phys. Chem. C* 112 (2008) 20114–20117, <https://doi.org/10.1021/jp808878p>.
- [5] V. Leonov, R.J.M. Vullers, Wearable electronics self-powered by using human body heat: the state of the art and the perspective, *J. Renew. Sustain. Energy* 1 (2009) 062701, <https://doi.org/10.1063/1.3255465>.
- [6] Z.L. Wang, Energy harvesting for self-powered nanosystems, *Nano Res* 1 (2008) 1–8, <https://doi.org/10.1007/s12274-008-8003-x>.
- [7] S. Saha, V. Gupta, Influence of surface defects in ZnO thin films on its biosensing response characteristic, *J. Appl. Phys.* 110 (2011) 064904, <https://doi.org/10.1063/1.3633212>.
- [8] N. Batra, M. Tomar, V. Gupta, Biosensors and Bioelectronics ZnO – CuO composite matrix based reagentless biosensor for detection of total cholesterol, *Biosens. Bioelectron.* 67 (2015) 263–271, <https://doi.org/10.1016/j.bios.2014.08.029>.
- [9] Y. Zhang, T.R. Nayak, H. Hong, W. Cai, Biomedical applications of zinc oxide nanomaterials, *Curr. Mol. Med.* 13 (2013) 1633–1645, <https://doi.org/10.2174/1566524013666131111130058>.
- [10] M. Israr-Qadir, S. Jamil-Rana, O. Nur, M. Willander, Zinc Oxide-Based Self-Powered potentiometric chemical sensors for biomolecules and metal ions, *Sensors* (2017) 17, <https://doi.org/10.3390/s17071645>.
- [11] J.T. Chen, J. Wang, R.F. Zhuo, D. Yan, J.J. Feng, F. Zhang, P.X. Yan, The effect of Al doping on the morphology and optical property of ZnO nanostructures prepared by hydrothermal process, *Appl. Surf. Sci.* 255 (2009) 3959–3964, <https://doi.org/10.1016/j.apsusc.2008.10.086>.
- [12] A.A.M. Ralib, O. Mortada, J.C. Orianges, A. Crunteanu, M. Chatras, A.N. Nordin, Enhanced piezoelectric properties of aluminum doped zinc oxide thin film for surface acoustic wave resonators on a CMOS platform, *J. Mater. Sci. Mater. Electron.* 28 (2017) 9132–9138, <https://doi.org/10.1007/s10854-017-6647-6>.
- [13] S. Hartner, M. Ali, C. Schulz, M. Winterer, H. Wiggers, Electrical properties of aluminum-doped zinc oxide (AZO) nanoparticles synthesized by chemical vapor synthesis, *Nanotechnology* 20 (2009) 445701, <https://doi.org/10.1088/0957-4484/20/44/445701>.
- [14] X. Jiang, F.L. Wong, M.K. Fung, S.T. Lee, X. Jiang, Aluminum-doped Zinc Oxide Films as Transparent Conductive Electrode for Organic Light-Emitting Devices Aluminum-Doped Zinc Oxide Films as Transparent Conductive Electrode for Organic Light-Emitting Devices vol. 1875, (2005), pp. 2001–2004, <https://doi.org/10.1063/1.1605805>.
- [15] S.-J. Young, Y.-H. Liu, Field emission properties of Al-doped ZnO nanosheet based on field emitter device with UV exposure, *RSC Adv.* 7 (2017) 14219–14223, <https://doi.org/10.1039/C7RA01236E>.
- [16] X. Zhao, H. Shen, Y. Zhang, X. Li, X. Zhao, M. Tai, J. Li, J. Li, X. Li, H. Lin, Aluminum-doped zinc oxide as highly stable electron collection layer for perovskite solar cells, *ACS Appl. Mater. Interfaces* 8 (2016) 7826–7833, <https://doi.org/10.1021/acsami.6b00520>.
- [17] J.H. Kim, S. Kwon, S. Na, Y. Yoo, T. Seong, Inverted organic solar cells fabricated with room-temperature-deposited transparent multilayer electrodes 38 (2017), pp. 856–860, <https://doi.org/10.1002/bkcs.11183>.
- [18] N.K. Elumalai, A. Mahmud, H. Sun, D. Wang, K.H. Chan, M. Wright, C. Xu, A. Uddin, Organic Solar Cells with Near 100 % Ef Fi Ciency Retention after Initial Burn-In Loss and Photo-Degradation vol. 636, (2017), pp. 127–136, <https://doi.org/10.1016/j.tsf.2017.05.031>.
- [19] Y. Hu, Y. Zhang, C. Xu, L. Lin, R.L. Snyder, Z.L. Wang, Self-powered system with wireless data transmission, *Nano Lett.* 11 (2011) 2572–2577, <https://doi.org/10.1021/nl201505c>.
- [20] N.S. Hudak, G.G. Amatucci, Small-scale energy harvesting through thermoelectric, vibration, and radiofrequency power conversion, *J. Appl. Phys.* 103 (2008) 1–24, <https://doi.org/10.1063/1.2918987>.
- [21] J. Briscoe, Nanostructured Piezoelectric Energy Harvesters, I, Springer Briefs in Materials, London UK, 2014, <https://doi.org/10.1007/978-3-319-09632-2>.
- [22] Z.L. Wang, W. Wu, Nanotechnology-enabled energy harvesting for self-powered micro-/nanosystems, *Angew Chem. Int. Ed. Engl.* 51 (2012) 11700–11721, <https://doi.org/10.1002/anie.201201656>.
- [23] N. Geetha, M. Jayachandran, J.S. Kissinger, A. Ayeshamariam, S. Sivarjanani, M. Valan Arasu, ZnO doped oxide materials: mini review, *Fluid Mech. Open Access* 03 (2017) 1000141, <https://doi.org/10.4172/2476-2296.1000141>.
- [24] J. Briscoe, S. Dunn, Piezoelectric nanogenerators - a review of nanostructured piezoelectric energy harvesters, *Nanomater. Energy* 14 (2014) 15–29, <https://doi.org/10.1016/j.nanoen.2014.11.059>.
- [25] F.S. Tsai, S.J. Wang, Enhanced sensing performance of relative humidity sensors using laterally grown ZnO nanosheets, *Sensor. Actuator. B Chem.* 193 (2014) 280–287, <https://doi.org/10.1016/j.snb.2013.11.069>.
- [26] J. Chiang, S. Tsai, Characteristics of Al-doped ZnO nanorods synthesized by the hydrothermal process at low temperature, *IEEE Trans. Power Electron.* (2013) 502–504.
- [27] X.H. Wang, L.Q. Huang, L.J. Niu, R.B. Li, D.H. Fan, F.B. Zhang, Z.W. Chen, X. Wang, Q.X. Guo, The impacts of growth temperature on morphologies, compositions and optical properties of Mg-doped ZnO nanomaterials by chemical vapor deposition, *J. Alloy. Comp.* 622 (2015) 440–445, <https://doi.org/10.1016/j.jallcom.2014.10.077>.
- [28] T. Tynell, M. Karppinen, Atomic layer deposition of ZnO: a review, *Semicond. Sci. Technol.* 29 (2014) 043001, <https://doi.org/10.1088/0268-1242/29/4/043001>.
- [29] L. Vayssieres, Growth of arrayed nanorods and nanowires of ZnO from aqueous solutions, *Adv. Mater.* 15 (2003) 464–466, <https://doi.org/10.1002/adma.200390108>.
- [30] J. Dutta, S. Baruah, J. Dutta, Hydrothermal growth of ZnO nanostructures, *Sci. Technol. Adv. Mater.* 10 (2009) 013001, <https://doi.org/10.1088/1468-6996/10/1/013001>.
- [31] Y.W. Koh, M. Lin, C.K. Tan, Y.L. Foo, K.P. Loh, Self-Assembly and Selected Area Growth of Zinc Oxide Nanorods on Any Surface Promoted by an Aluminum Precoat, (2004), pp. 11419–11425.
- [32] T.H. Hsieh, J.Y. Chen, C.W. Huang, W.W. Wu, Observing growth of nanostructured ZnO in liquid, *Chem. Mater.* 28 (2016) 4507–4511, <https://doi.org/10.1021/acs.chemmater.6b02040>.
- [33] R. Parize, J. Garnier, O. Chaix-Pluchery, C. Verrier, E. Appert, V. Consonni, Effects of hexamethylenetetramine on the nucleation and radial growth of ZnO nanowires by chemical bath deposition, *J. Phys. Chem. C* 120 (2016) 5242–5250, <https://doi.org/10.1021/acs.jpcc.6b00479>.
- [34] D. Polsongkram, P. Chamminok, S. Pukird, L. Chow, O. Lupan, G. Chai, H. Khallaf, S. Park, A. Schulte, Effect of synthesis conditions on the growth of ZnO nanorods via hydrothermal method, *Phys. B Condens. Matter* 403 (2008) 3713–3717, <https://doi.org/10.1016/j.physb.2008.06.020>.
- [35] Y. Sun, D.J. Riley, M.N.R. Ashford, Mechanism of ZnO nanotube growth by hydrothermal methods on ZnO film-coated Si substrates, *J. Phys. Chem. B* 110 (2006) 15186–15192, <https://doi.org/10.1021/jp062299z>.
- [36] W. Feng, B. Wang, P. Huang, X. Wang, J. Yu, C. Wang, Wet chemistry synthesis of ZnO crystals with hexamethylenetetramine(HMTA): understanding the role of HMTA in the formation of ZnO crystals, *Mater. Sci. Semicond. Process.* 41 (2016) 462–469, <https://doi.org/10.1016/j.mssp.2015.10.017>.
- [37] S. Guillemin, L. Rapenne, V. Consonni, H. Roussel, E. Sarigiannidou, N. De Lyon, U. De Lyon, I. Lyon, B. Blaise, Formation Mechanisms of ZnO Nanowires: the Crucial Role of Crystal Orientation and Polarity Georges Bre M, (2013).
- [38] K.M. McPeak, T.P. Le, N.G. Britton, Z.S. Nickolov, Y. a Elabd, J.B. Baxter, Chemical bath deposition of ZnO nanowires at near-neutral pH conditions without hexamethylenetetramine (HMTA): understanding the role of HMTA in ZnO nanowire growth, *Langmuir* 27 (2011) 3672–3677, <https://doi.org/10.1021/la105147u>.
- [39] R. Wahab, S.G. Ansari, Y.S. Kim, M. Song, H.S. Shin, The role of pH variation on the growth of zinc oxide nanostructures, *Appl. Surf. Sci.* 255 (2009) 4891–4896, <https://doi.org/10.1016/j.apsusc.2008.12.037>.
- [40] G. Murillo, I. Rodriguez-Ruiz, J. Esteve, Selective area growth of high-quality ZnO nanosheets assisted by patternable AlN seed layer for wafer-level integration, *Cryst. Growth Des.* 16 (2016) 5059–5066, <https://doi.org/10.1021/acs.cgd.6b00661>.
- [41] G. Murillo, H. Lozano, J. Kases-Utrera, M. Lee, J. Esteve, Improving morphological quality and uniformity of hydrothermally grown ZnO nanowires by surface activation of catalyst layer, *Nanoscale Res. Lett* 12 (2017) 51, <https://doi.org/10.1186/s11671-017-1838-x>.
- [42] S.K. Das, S.N. Sahoo, S.N. Sarangi, P.K. Sahoo, Substrate effect of hydrothermally grown ZnO nanorods and its luminescence properties, *J. Exp. Nanosci.* 8 (2013) 382–388, <https://doi.org/10.1080/17458080.2012.702931>.
- [43] M. Van Schilfgaarde, A. Sher, A.B. Chen, Theory of AlN, GaN, InN and their alloys, *J. Cryst. Growth* 178 (1997) 8–31, [https://doi.org/10.1016/S0022-0248\(97\)00073-0](https://doi.org/10.1016/S0022-0248(97)00073-0).
- [44] S. Fukumoto, T. Hookabe, H. Tsubakino, H. Tsubakino, Hydrolysis behavior of aluminum nitride in various solutions, *J. Mater. Sci.* 35 (2000) 2743–2748, <https://doi.org/10.1023/A:1004718329003>.
- [45] A.A. Al-Ghamdi, O.A. Al-Hartomy, M. El Okr, A.M. Nawar, S. El-Gazzar, F. El-Tantawy, F. Yakuphanoglu, Semiconducting properties of Al doped ZnO thin films, *Spectrochim. Acta Part A Mol. Biomol. Spectrosc.* 131 (2014) 512–517, <https://doi.org/10.1016/j.saa.2014.04.020>.
- [46] H. Morkoç, Ü. Özgür, General properties of ZnO, *Zinc Oxide*, 2009, pp. 1–76, <https://doi.org/10.1002/9783527623945.ch1>.
- [47] F. Güell, P.R. Martínez-Alanis, Tailoring the Green, Yellow and Red defect emission bands in ZnO nanowires via the growth parameters, *J. Lumin.* 210 (2019) 128–134, <https://doi.org/10.1016/j.jlumin.2019.02.017>.
- [48] A. Vanaja, G.V. Ramaraju, K. Srinivasa Rao, Structural and optical investigation of Al doped ZnO nanoparticles synthesized by Sol-gel process, *Indian J. Sci. Technol.* 9 (2016) 1–6, <https://doi.org/10.17485/ijst/2016/v9i12/87013>.
- [49] S. Yun, J. Lee, J. Yang, S. Lim, Hydrothermal synthesis of Al-doped ZnO nanorod arrays on Si substrate, *Phys. B Condens. Matter* 405 (2010) 413–419, <https://doi.org/10.1016/j.physb.2009.08.297>.
- [50] B.K. Sharma, N. Khare, Stress-dependent band gap shift and quenching of defects in Al-doped ZnO films, *J. Phys. D Appl. Phys.* 43 (2010) 465402, <https://doi.org/10.1088/0022-3727/43/46/465402>.
- [51] S. Käbisch, M.A. Gluba, C. Klimm, S. Krause, N. Koch, N.H. Nickel, Polarity driven morphology of zinc oxide nanostructures, *Appl. Phys. Lett.* 103 (2013) 103106, <https://doi.org/10.1063/1.4820410>.
- [52] X. Han, H. He, Q. Kuang, X. Zhou, X. Zhang, T. Xu, Controlling Morphologies and Tuning the Related Properties of Nano/Microstructured ZnO Crystallites Controlling Morphologies and Tuning the Related Properties of Nano/Microstructured ZnO, (2009), pp. 584–589, <https://doi.org/10.1021/jp808233e>.
- [53] V. Gaddam, R.R. Kumar, M. Parmar, G.R.K. Yaddanapudi, M.M. Nayak, K. Rajanna, Morphology controlled synthesis of Al doped ZnO nanosheets on Al alloy substrate by low-temperature solution growth method, *RSC Adv.* 5 (2015) 13519–13524, <https://doi.org/10.1039/C4RA14049D>.
- [54] P.-C. Yao, S.-T. Hang, Y.-C.Y.-S. Lin, W.-T. Yen, Y.-C.Y.-S. Lin, Optical and electrical characteristics of Al-doped ZnO thin films prepared by aqueous phase deposition, *Appl. Surf. Sci.* 257 (2010) 1441–1448, <https://doi.org/10.1016/j.apsusc.2010.08.064>.

- [55] L.M. Svedberg, K.C. Arndt, M.J. Cima, Corrosion of aluminum nitride (AlN) in aqueous cleaning solutions, *J. Am. Ceram. Soc.* 83 (2000) 41–46, <https://doi.org/10.1111/j.1151-2916.2000.tb01145.x>.
- [56] J. Li, M. Nakamura, S. Takashi, K. Matsumaru, Ishizaki, hydrolysis of aluminum nitride powders in moist air, *Adv. Technol. Mater. Process.* 7 (2005) 37–42, <https://doi.org/10.2240/azojomo0111>.
- [57] C. Ye, Y. Bando, G. Shen, D. Golberg, Thickness-Dependent photocatalytic performance of ZnO nanoplatelets, *J. Phys. Chem. B* 110 (2006) 15146–15151, <https://doi.org/10.1021/jp061874w>.
- [58] T. Yingsamphancharoen, P. Nakarungsee, T.S. Herng, J. Ding, I.M. Tang, S. Thongmee, Ferromagnetic behavior due to Al<sup>3+</sup> doping into ZnO nanorods, *J. Magn. Magn. Mater.* 419 (2016) 274–281, <https://doi.org/10.1016/j.jmmm.2016.06.025>.
- [59] G. Amin, M.H. Asif, A. Zainelabdin, S. Zaman, O. Nur, M. Willander, Influence of pH, precursor concentration, growth time, and temperature on the morphology of ZnO nanostructures grown by the hydrothermal method, *J. Nanomater.* 2011 (2011), <https://doi.org/10.1155/2011/269692>.
- [60] R.D. Shannon, Revised effective ionic radii and systematic studies of interatomic distances in halides and chalcogenides, *Acta Crystallogr. A* 32 (1976) 751–767, <https://doi.org/10.1107/S0567739476001551>.
- [61] G. Murillo, A. Blanquer, C. Vargas-Estevez, L. Barrios, E. Ibáñez, C. Nogués, J. Esteve, Electromechanical nanogenerator-cell interaction modulates cell activity, *Adv. Mater.* 29 (2017) 1605048, <https://doi.org/10.1002/adma.201605048>.
- [62] Z.L. Wang, X.D. Wang, J.H. Song, J. Liu, Direct-current nanogenerator driven by ultrasonic waves, *Science* 316 (2007) 102–105, <https://doi.org/10.1126/science.1139366>.
- [63] G. Murillo, M. Lee, C. Xu, G. Abadal, Z.L. Wang, Z. Lin, Hybrid resonant energy harvester integrating ZnO NWs with MEMS for enabling zero-power wireless sensor nodes, *Nano Commun. Netw.* 2 (2011) 235–241, <https://doi.org/10.1016/j.nancom.2011.10.001>.
- [64] K. Famm, B. Litt, K.J. Tracey, E.S. Boyden, M. Slaoui, A jump-start for electroceuticals, *Nature* 496 (2013) 159 <https://doi.org/10.1038/496159a>.
- [65] K. Birmingham, V. Gradinaru, P. Anikeeva, W.M. Grill, V. Pivov, B. McLaughlin, P. Pasricha, D. Weber, K. Ludwig, K. Famm, Bioelectronic medicines: a research roadmap, *Nat. Rev. Drug Discov.* 13 (2014) 399–400, <https://doi.org/10.1038/nrd4351>.
- [66] Y. Zi, F. Hu, W. Wu, Z.L. Wang, R. Liu, W. Ding, H. Zou, C. Wu, W. Peng, R. Yu, X. Li, Piezo-photonic effect on selective electron or hole transport through depletion region of vis-NIR broadband photodiode, *Adv. Mater.* 29 (2017) 1701412, <https://doi.org/10.1002/adma.201701412>.
- [67] W. Peng, C. Xu, G. Dai, X. Li, A.C. Wang, Z.L. Wang, S.-L. Zhang, Y. Zhang, H. Zou, Y. Ding, S.L. Zhang, Dramatically enhanced broadband photodetection by dual inversion layers and Fowler–Nordheim tunneling, *ACS Nano* (2019), <https://doi.org/10.1021/acsnano.8b08998>.
- [68] C.-Y. Lin, Y.-H. Lai, H.-W. Chen, J.-G. Chen, C.-W. Kung, R. Vittal, K.-C. Ho, Highly efficient dye-sensitized solar cell with a ZnO nanosheet-based photoanode, *Energy Environ. Sci.* 4 (2011) 3448, <https://doi.org/10.1039/c0ee00587h>.
- [69] Q. Rui, K. Komori, Y. Tian, H. Liu, Y. Luo, Y. Sakai, Electrochemical biosensor for the detection of H<sub>2</sub>O<sub>2</sub> from living cancer cells based on ZnO nanosheets, *Anal. Chim. Acta* 670 (2010) 57–62, <https://doi.org/10.1016/j.aca.2010.04.065>.

**Dr. Gonzalo Murillo** received his Electronic Engineering Degree from the Universidad de Granada (Spain) in 2007 and his PhD at the Electronic Engineering Department of the Universitat Autònoma de Barcelona (UAB) in 2011. Then, he worked at the International Iberian Nanotechnology Laboratory (INL) in Portugal. He joined the Microelectronic Institute of Barcelona (IMB-CNM, CSIC). In June 2016, he was named “Most Novel Innovator in Europe” by the MIT Technology Review. In 2017, he founded a start-up company called Energiot Devices SL ([www.energiot.com](http://www.energiot.com)). He has published 35 papers, participated in around 30 research projects, and attended more than 55 international conferences. He was professor at the Universidad Autònoma de Barcelona. He has supervised 10 Master and graduate students and three PhD students. He was visiting researcher at Georgia Tech (USA), Infineon (Germany), Minatec (France), DTU (Denmark) and INHA University (Korea). His main research is focused on smart nanomaterials and microdevices for energy harvesting and bioelectronic applications.



**Edgardo León Salguero** (1984) received his degree as Mechanical engineering by the Hermosillo Technological Institute (ITH) in Hermosillo, Mexico in 2008. And Materials Sciences Master degree by Centro de investigación de Materiales Avanzados (CIMAV) in 2011. He is currently conducting his doctoral research in Posgrado de Nanotecnología at

Universidad de Sonora, visiting student at the IMB-CNM (CSIC), His research interest focus on Piezoelectrics materials for energy harvesting and flexible electronics.



**Dr. Paulina R. Martínez-Alanis** obtained her PhD in Science on the field of Chemistry at Universidad Nacional Autónoma de México (UNAM) in 2012. Currently, she is working on nanostructured materials, mainly ZnO, at the Universitat de Barcelona (UB) and its applications in electronics, sensors, and catalysis. She is also interested in the activation and conversion of CO<sub>2</sub>, O<sub>2</sub>, N<sub>2</sub> into feedstock products and H<sub>2</sub> production.



**Josefina Alvarado Rivera** is a CONACyT Fellow researcher at the Physics Department or the University of Sonora in Mexico since 2014. She received its Ph.D. degree in Materials Science from The Center for Research and Advanced Studies in 2010. Her research interest focus on chemical synthesis of photoluminescent nanoparticles, carbon dots, nanocomposites and rare-earth doped tellurite glasses for light-emitting diodes applications.



**Dr. Frank Güell** received in 2005 the PhD degree in Physics from Universitat de Barcelona (UB). His successful doctorate work (14 papers) warranted him a Postdoctoral Juan de la Cierva Fellowship at Universitat Rovira i Virgili (URV) in 2006. After that, he became Assistant Professor at UB where he is Associate Professor of Electronics since 2011. During his PhD and afterwards he joined several times the Max-Born-Institute for Nonlinear Optics and Ultrafast Spectroscopy (MBI) in Berlin, Germany. During the academic year 2013–2014, he was Visiting Scholar at the Department of Electrical and Computer Engineering of the University of California San Diego (UCSD) in San Diego, USA. In addition he has pronounced 60 lectures at international conferences, 10 as invited speaker. He has also been invited to impart research seminars to universities throughout the world. His general area of research is in the growth and study of semiconductors such as wide band gap materials and nanostructures using optical spectroscopy and other characterization techniques. His research interests also include nanophotonics and photocatalysis, and he's coauthored about 50 papers in scientific journals.

